Mg/Ca from mussel shells rather than δ18w O as a promising temperature proxy for hydrothermal vent ecosystems

V. Mouchi, K. Nedoncelle, O. Bruguier, Z. Garmirian, N. Le Bris, F. Lartaud

Deep–Sea Research I 219 (2025) 104485

Contents lists available at ScienceDirect

Deep-Sea Research Part I

journal homepage: www.elsevier.com/locate/dsri

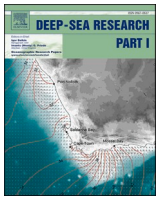

Mg/Ca from mussel shells rather than $\delta^{18}O$ as a promising temperature proxy for hydrothermal vent ecosystems

V. Mouchi [a,b], K. Nedoncelle [c], O. Bruguier [d], Z. Garmirian [c], N. Le Bris [c,e], F. Lartaud [c,*]

[a] Sorbonne Université, CNRS, UMR 7144, Station Biologique de Roscoff, Place Georges Teissier, 29680, Roscoff, France
[b] Current address: CNRS UMR 6566 CReAAH (Centre de Recherche en Archéologie, Archéosciences, Histoire), Université de Rennes, Campus Beaulieu, 263 avenue Général Leclerc, bât. 24-25 -CS74205, 35042, Rennes Cedex, France
[c] Sorbonne Université, CNRS, Laboratoire d'Ecogéochimie des Environnements Benthiques, LECOB, Observatoire Océanologique, Banyuls-sur-mer, F-66650, France
[d] Géosciences Montpellier, CNRS UMR 5243, Université Montpellier, CC60, F-34095, Montpellier, CEDEX 05, France
[e] Sorbonne Université, MNHN, CNRS, SU, EPHE-PSL, UA, Institut de Systématique, Évolution, Biodiversité (ISYEB), 12 rue Buffon, F-75005, Paris, France

ARTICLE INFO

Keywords:
Deep-sea hydrothermal habitat
Bathymodiolus shells
Magnesium-calcium ratio
Oxygen stable isotopes
Paleothermometer

ABSTRACT

Minor and trace metal fluctuations in biogenic carbonates have been demonstrated to be important potential environmental tracers in coastal areas, but remained poorly studied in deep-sea environments. For the first time, this study assesses the use of Mg/Ca signal as a thermometer proxy in hydrothermal vent ecosystems together with the analysis of oxygen stable isotope composition. *Bathymodiolus azoricus* and *B. thermophilus* mussels were collected at three hydrothermal vent fields from the mid-Atlantic ridge (Rainbow, Menez Gwen) and the East Pacific Rise (EPR 9°50N), presenting contrasted temperature and chemical habitat conditions. The variation of Mg/Ca was analysed via LA-ICP-MS and is revealed suitable to reconstruct temperature variations in these ecosystems, presumably due to stable Mg compositions of the seawater surrounding hydrothermal systems. Temperature anomalies inferred from Mg/Ca ratios can be good tracers of fluid pulses. Important fluid emissions appear however to generate major growth cessation in shell mineralization. Temperatures inferred from Isotope Ratio Mass Spectrometry (IRMS) $\delta^{18}O$ analyses systematically underestimated the measured values in the environment. The isotopic disequilibrium is likely due to pH fluctuations in the mussel habitat, in the vicinity of vent fluid discharges, and/or interactions with the symbiotic chemosynthetic bacteria. Those results will first benefit to the ecological study of deep-sea mussels, but also provide a promising contribution for the study of the environmental dynamic in hydrothermal systems at short (daily) to long-term (pluri-annual) scales, recorded in the calcite material of bivalves.

1. Introduction

As they build carbonate structures from ions sampled from the surrounding environment, mollusc shells are used as a natural recorder of past and present climate and environmental parameters (Dodd, 1965; Klein et al., 1996; Huyghe et al., 2015). The shells are formed by incremental growth, preventing the destruction of previously secreted parts, which allows the evaluation of the environmental variations throughout the life of an organism (Schöne, 2008). Historically, this type of study started with the measurements of oxygen isotope ratios ($\delta^{18}O$; Urey, 1947), which are commonly used as a proxy for seasonal temperature reconstructions in a variety of environments such as freshwater (Dettman et al., 1999; Goodwin et al., 2019) and coastal (Klein et al., 1996; Lartaud et al., 2010a; Welsh et al., 2011) settings. However, several limitations have been identified for the use of this proxy. First, $\delta^{18}O$ in shells, not only changes with temperature, but also with the seawater $\delta^{18}O$ composition ($\delta^{18}O_w$), which covaries with salinity, and is not properly constrained particularly in coastal environments (Rohling, 2000). Second, strong disequilibrium between seawater and biogenic carbonates has been observed in numerous taxa (Aharon, 1991; Daëron et al., 2019). Although these disequilibria, called 'vital effects' (*i.e.*, resulting from kinetic and physiological impacts during biomineralization), appear limited in mollusc biominerals (Aharon, 1991; Welsh et al., 2011), strong isotopic anomalies have been recently highlighted in juvenile oyster shells, likely due to kinetic effects during this period of rapid growth (Huyghe et al., 2020), and for deep-sea oysters (Wisshak et al., 2009; Huyghe et al., 2022).

As alternative proxies for temperature, elemental ratios (*i.e.*, Mg/Ca

* Corresponding author.
E-mail address: franck.lartaud@obs-banyuls.fr (F. Lartaud).

https://doi.org/10.1016/j.dsr.2025.104485
Received 27 January 2025; Received in revised form 3 March 2025; Accepted 10 March 2025
Available online 12 March 2025

in calcite and Sr/Ca in aragonite) have been investigated and salinity fluctuations appear to have a weak impact, if any (Vander Putten et al., 2000; Mouchi et al., 2013). However, differences in Mg uptake from natural sites or aquarium-based rearing experiments have been reported for mytilids (Klein et al., 1996; Vander Putten et al., 2000; Freitas et al., 2008; Wanamaker et al., 2008; Tanaka et al., 2019), oysters (Surge and Lohmann, 2008; Mouchi et al., 2013; Tynan et al., 2017) and pectinids (Freitas et al., 2012). In coastal waters, although some Mg/Ca-temperature relationships appear very similar depending on the environmental settings (Mouchi et al., 2018), it has been reported that Mg/Ca variations in seawater caused by rapid salinity changes and Mg supply from continental rock alteration can mask the temperature effect on the Mg uptake in shell carbonates (Dodd, 1965; Wanamaker et al., 2008). Vital effects may also impact elemental uptake (Carré et al., 2006; Schöne et al., 2011; Mouchi et al., 2013).

In deep-sea environments, few studies were dedicated to the analyses of metal concentrations in calcifying materials. Most focus has been on investigations in cold-water coral skeletons, where Mg/Ca ratio has been demonstrated to be an unreliable paleothermometer proxy (Lopez-Correa et al., 2010; Robinson et al., 2014). Although potentially in the vicinity of hydrothermal systems, those corals are not directly associated with vent fluids, in contrast to chemosynthetic bivalve species such as hydrothermal mussels. The geochemical proxies studied in bivalve shells from hydrothermal vents focused on stable isotopes, such as the $\delta^{13}C$ to reconstruct chemosynthetic pathways (Nedoncelle et al., 2014) or carbon sources (Naraoka et al., 2008; Lietard and Pierre, 2009; Lartaud et al., 2010b, 2011), and the use of minor and trace elements for the characterization of heavy metals present in the mixing zone (Kádár et al., 2005; Cravo et al., 2008), or the study of metal detoxification processes (Demina et al., 2013). The studies thus focused on trace metals typically associated with hydrothermal systems (*e.g.*, Fe, Mn, Zn, Cu, Cd), and other classical elements used in shallow-water biological archives were not considered, particularly Mg/Ca as end-member hydrothermal fluids are severely depleted in magnesium (Corliss et al., 1979; Charlou et al., 2002). Although no precise calibrations were performed, previous works from Rio et al. (1988) suggest that the Mg/Ca and Sr/Ca ratios in hydrothermal bivalve shells are consistent with those of the ambient seawater. Shirai et al. (2008) studied the distribution of Mg/Ca in *Bathymodiolus* shells in depth but they focused on the inner aragonite nacreous layer, which is generally not used for environmental reconstruction in shallow-water species. Indeed, sclerochemistry in bivalve shells is mostly performed on the outer calcite prismatic layer, an area associated with higher growth rates leading to better time-resolution sampling.

Mytilids from the genus *Bathymodiolus* are among the most successful colonizers of vent environments and often dominate the biomass of hydrothermal communities (Van Dover, 2000). *Bathymodiolus* habitat is characterized by fluctuation of the environmental parameters, including pH, oxygen and temperature, resulting from hydrothermal fluid mixing with the background cold-seawater (Le Bris and Duperron, 2010; Le Bris et al., 2019). The temperatures range from strictly deep seawater temperature (i.e., 2–4 °C) to fluid-related (reaching 10–15 °C), associated to the influence of tides on the deep-sea current regime and fluid vent flux (Johnson et al., 1994; Tivey et al., 2002; Nedoncelle et al., 2015; Lelièvre et al., 2017). This range seems to be maintained for long time periods, only disrupted by occasional anomalies (Scheirer et al., 2006; Khripounoff et al., 2008; Mullineaux et al., 2012).

The purpose of this paper is to investigate the potential of using Mg/Ca and $\delta^{18}O$ in deep-sea mussel shells from hydrothermal vents. Particularly, the study focuses on the variations of these proxies during growth, to investigate the record of the vent dynamics. Using *Bathymodiolus azoricus* (von Cosel et al., 1999) and *B. thermophilus* (Kenk and Wilson, 1985) growing at five contrasting temperature vent habitats from three sites, the evolution of Mg/Ca was measured by LA-ICP-MS and $\delta^{18}O$ by IRMS and compared to the temperature monitored in the mussel habitat.

2. Methods

2.1. Sampling area

Mussel shells were collected at three hydrothermal vent sites from the Mid-Atlantic Ridge (MAR) and the East Pacific Rise (EPR): Rainbow (36°13.8′N-33°54.1′W, 2275 m), Menez Gwen (37°50.6′N-31°31.2′W, 815 m) and EPR 9°50′N (09°47.3′N-104°17.0′W, 2513m). Rainbow end-member fluids formed in ultramafic basement are characterized by high methane and hydrogen contents but also high metal concentrations. Menez Gwen fluids are also characterized by methane and hydrogen gases but depleted in metals (Charlou et al., 2002). The average temperature in the mussel habitat is higher at Menez Gwen (10.9 °C) than at Rainbow (3.7 °C), due to the greater depth of the latter (Desbruyères et al., 2001). EPR vent fluids exhibit important free sulphide but low methane and hydrogen concentrations.

Live *B. azoricus* from Rainbow were collected during the MoMAR-DREAM cruise (CNRS, R/V L'Atalante, August–September 2008) using the Victor 6000 ROV and then dissected onboard. Two areas of collection were selected as described in Nedoncelle et al. (2014): Z1 zone, which corresponds to mussels living at the basis of a sulphide structure about 1 m-high in the immediate vicinity of a small spire-type active chimney; and Z3 zone, which harbours a higher density of mussels and is located further away from the chimney on the top of the rocky structure at ~1 m above Z1 (Fig. 1).

At Menez Gwen, live *B. azoricus* shells were collected during the MenezMAR cruise (MARUM, R/V *Meteor*, September-October 2010) using the Quest 4000 ROV. Mussels were sampled at Cage Site (CS), from a small discretely distributed mussel patch at the top of a hydrothermal area presenting some active diffuse vents, and along the flank of the White Flame (WF) site fully colonized by mussels and dominated by a large active white smoker (Fig. 1).

The live *B. thermophilus* from EPR 9°50N were collected during the MESCAL-1 cruise (UPMC, R/V *L'Atalante*, April–May 2010) with the Nautile submersible in a ~50 m^2 mussel bed at V-Vent site (MES), a diffuse vent area on the basaltic seafloor (Fig. 1) (see Nedoncelle et al., 2013 for more details).

2.2. Shell preparation and observation

Bathymodiolus shells are formed of an aragonite lower (inner) layer and a calcite upper (outer) layer (Carter, 1990; Nedoncelle et al., 2013). Geochemical analyses were performed on the calcite upper layer, since calcite is less sensitive to alteration and dissolution than aragonite in those environments, and preserves the pristine signal from diagenetic alterations (Lutz et al., 1994). Shells were sectioned along the maximum growth axis and mounted on epoxy blocks. Sections were ground flat using 180, 400 and 800 grit powder with distilled water and then polished using Al_2O_3 powder at 3, 1 and 0.3 μm. A Mutvei treatment (Schöne et al., 2005) was used to reveal growth structures (Fig. 2A). Major growth lines were identified as growth lines present both in the upper calcitic and lower aragonitic layers, often accompanied with shell distortion on the external surface (Schöne and Giere, 2005). Part of the data were from Nedoncelle et al. (2014).

During the MenezMAR cruise, shells from Cage Site at Menez Gwen were stained with calcein following the protocol described in Nedoncelle et al. (2013) and recovered after 10 days. Despite the success of staining (100 % of the shells revealed the calcein line), no growth was observed during the 10 days mark and recapture period (Supplementary Fig. S1), in contrast to the *B. thermophilus* used in Nedoncelle et al. (2013).

2.3. LA-ICP-MS analyses

Four shells from Rainbow (1 for Zone 1 and 3 for Zone 3, with sizes ranging from 34 to 52 mm), four shells from Menez Gwen vent sites (2

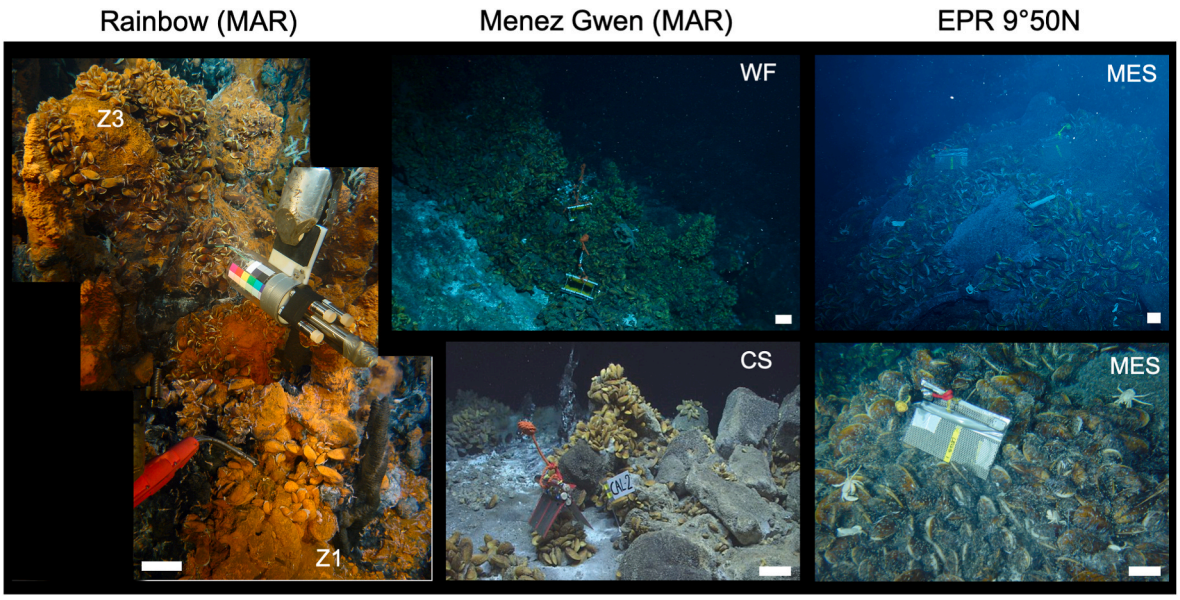

Fig. 1. Sampling areas for the three hydrothermal vent sites. At Rainbow, shells were collected from two micro-habitats: Z1, where mussels lived close to the active chimney (in black), and Z3, corresponding to a denser mussel patch ~1m above (© Ifremer – MoMARDREAM). At Menez Gwen, shells originated from two locations: White Flame (WF) and Cage Site (CS). For CS, the shells collected are the ones below the red autonomous probe (© Marum – MenezMAR). At EPR 9°50N, shells were collected in the V-Vent area (here called MES), around the yellow autonomous probe (© Ifremer – MESCAL-1). White scale bar is 10 cm. (For interpretation of the references to colour in this figure legend, the reader is referred to the Web version of this article.)

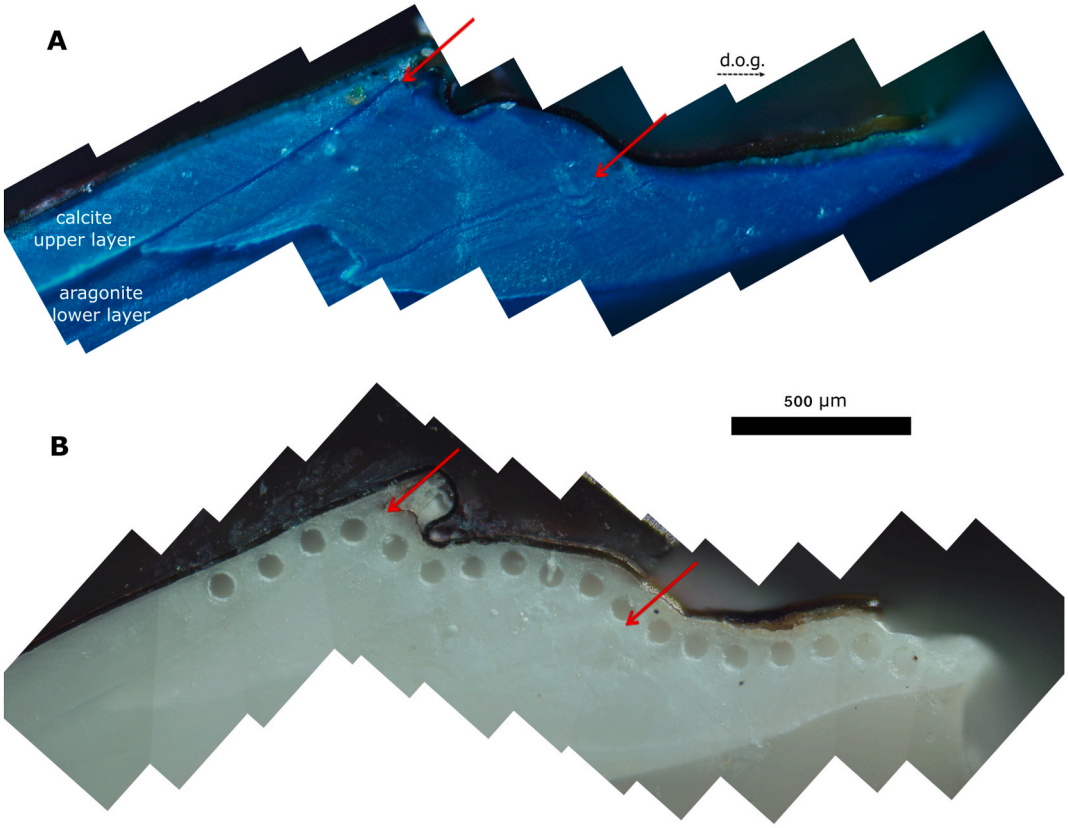

Fig. 2. Photographs of cross section of a *B. azoricus* shell (specimen Z3-116), at the ventral margin highlighting the details of the microstructures and growth increments revelation under Mutvei treatment (A), and the position of the LA-ICP-MS samplings (B). d.o.g. is direction of growth. Red arrows highlight the position of major growth lines. (For interpretation of the references to colour in this figure legend, the reader is referred to the Web version of this article.)

for Cage Site, previously stained with calcein, see above, and 2 for White Flame, with shell sizes from 46 to 84 mm), and two shells from EPR 9°50N (sizes of 154 and 170 mm) were analysed for Mg abundances. Before elemental analyses, the sections were repolished to remove the Mutvei solution and prevent any influence of this treatment on the chemical analyses. The shell sections were analysed by Laser Ablation-

Inductively Coupled-Plasma-Mass Spectrometry (LA-ICP-MS) with a Compex102 193 nm excimer laser (Lambda Physik) coupled to a sector field ICP-MS (Thermofinnigan Element XR) at Montpellier University (AETE-ISO platform of the OSU OREME). Measured elements were ^{24}Mg and ^{43}Ca as the internal standard to control the ablated volume. The laser was operated at a repetition rate of 7 Hz and an energy density of 12 J cm^{-2}. Each analysis was done as a single spot using a spot size of 51 μm (Fig. 2B) after a pre-ablation time of 1 s for surface cleaning and corresponds to a total acquisition time of 180 s with the first 120 s as background acquisition (gas blank). Data were normalized using the ^{43}Ca signal (internal standard) according to Longerich et al. (1996) and calibrated using NIST SRM 612 glass reference material (values after Pearce et al., 1997). Reproducibility of the values in the shell samples was also tested using the USGS MACS-3 carbonate reference material. Both reference materials were analysed every 10 measurements. Precision based on the analysis of the reference materials was approximately ±5 %.

2.4. Temperature reconstruction from Mg/Ca

Values of Mg/Ca were converted into temperatures using the equation from Vander Putten et al. (2000), established on the shell of the shallow water mussel *Mytilus edulis*:

$$Mg/Ca\ (mmol.\ mol^{-1}) = 0.70 * T(°C) - 0.63\ (r = 0.91)$$

This equation was chosen among the different equations existing for bivalve shells as it was established with a mytilid species, as *Bathymodiolus* (Mikkelsen et al., 2006), with a similar shell microstructure (*i.e.*, fibrous prismatic calcite layer) in the area investigated (Carter, 1980; Machado et al., 2009; Génio et al., 2012; Checa et al., 2014). Additionally, in the course of this study, the Mg/Ca measurement was performed with LA-ICP-MS, as in Vander Putten et al. (2000). This contrasts with the other temperature-Mg/Ca relationships published for *M. edulis* which were acquired by ICP-AES analyses (Klein et al., 1996; Wanamaker et al., 2008).

2.5. Oxygen isotope ratios

The remaining section of the shells was used for oxygen isotopes analysis. When possible we tried to use the same specimen already analysed for Mg/Ca. As some of them were broken during handling, we had to include additional shells. Shells were placed in a peroxide solution (H_2O_2 3.4 %) during 6–10 h at 60 °C to remove the periostracum and then rinsed with demineralized water before sampling the calcite outer layer for the oxygen isotopes ($\delta^{18}O$) analysis (see Nedoncelle et al., 2014). Shells were then drilled every 1 mm from the ventral margin to the hinge area along the maximum growth axis, with a Dremel device equipped with a 0.3 mm drill bit. The nacreous aragonite underlayer was carefully avoided to preclude any mineralogical effect on the isotopic values as aragonite is enriched in ^{18}O by 0.6 ‰ compared to calcite (Tarutani et al., 1969).

The collected calcium carbonate powders were acidified in 100 % H_3PO_4 at 90 °C under vacuum. The CO_2 produced was collected and analysed using a VG Instruments Isoprime mass spectrometer. Isotopic data are reported in the conventional delta (δ) notation relative to the Vienna Pee Dee Belemnite (V-PDB). The standard deviation for $\delta^{18}O$ values was ±0.1 ‰.

Seawater samples directly above the mussel bed were additionally collected during the dives for mussel collection at EPR 9°50N (MES) and Rainbow (Z1 and Z3). 20 mL of *in situ* water were sampled in airtight titanium syringes and analysed following the method of Pierre et al. (1994). The analyses were performed at the Institut d'Écologie et des Sciences de l'Environnement de Paris at Grignon. Seawater oxygen isotope compositions ($\delta^{18}O_w$) were obtained after CO_2-H_2O equilibration using an Isoprime mass spectrometer coupled to a Gilson X222 Micromass Aquaprep. Standard error for $\delta^{18}O_w$ was 0.15 ‰ and values expressed relative to SMOW reference.

2.6. Temperature reconstruction from $\delta^{18}O$

Based on the thermodynamic model for synthetic and biogenic carbonates, temperatures can be estimated from shell $\delta^{18}O$ and $\delta^{18}O_w$ measured in each habitat. We used the equation of Kim and O'Neil (1997):

$$1000 \times \ln(\alpha) = 18.03 \times (10^3 \times T^{-1}) - 32.42$$

where α represents the isotope fractionation factor:

$$\alpha = (1000 + \delta^{18}O_{shell}) / (1000 + \delta^{18}O_w)$$

In this last equation, both $\delta^{18}O_{shell}$ and $\delta^{18}O_w$ are expressed in ‰ SMOW. $\delta^{18}O_{shell}$ were converted from V-PDB to SMOW according to the equation of Coplen et al. (1983).

As no $\delta^{18}O_w$ were measured from habitats at Menez Gwen, and considering its proximity with Rainbow, we used the mean $\delta^{18}O_w$ value of Rainbow for temperature reconstructions from shells of Menez Gwen.

2.7. Temperature probes

In situ temperature measurements in mussel habitats were acquired at discrete locations in Rainbow (on both Z1 and Z3 areas), based on continuous records over 5 min for each analysis using a glass Ag/AgCl electrode coupled to a thermocouple (MICREL, France) (Fig. 1). Discrete measurements were also acquired at Menez Gwen (White Flame) by a temperature probe fixed to the sampling nozzle of the Kiel In Situ Pumping System (KIPS) (Meier et al., 2016; raw data pers. comm. C. Vidoudez). At Menez Gwen (Cage Site) and EPR 9°50N (V-Vent), autonomous probes (S2T6000, NKE) were used above the collected mussels (Fig. 1). The autonomous probes were deployed during 10 days at Menez Gwen (*i.e.*, during the staining experiment) on the mussel bed studied and recovered at the time of mussel sampling, with an acquisition every 5 min during this period. The deployment protocol of autonomous probes at EPR 9°50 was described in Nedoncelle et al. (2015). The probes monitored the habitat conditions during 10 days with a frequency of 2 measurements per hour.

2.8. Statistical analysis

Comparisons of isotopic and Mg compositions between shells were performed using Matlab (R2022a; www.mathworks.com) by applying the Kruskal and Wallis test (KW) followed by a *post hoc* test to discriminate the outlying groups (Tukey's honestly significant difference procedure; HSD). The KW test is used for comparison of more than two samples to infer if at least one sample is different from the others, whereas the HSD test determines which sample is different from the others. Before using this non-parametric test, the non-respect of the normality and homoscedasticity conditions were checked using the Kolmogorov-Smirnov and Levene tests, respectively. Shell Mg/Ca were compared using the correlation test of Spearman.

3. Results

3.1. Mg/Ca analysis

The Mg/Ca values range from 1.8 to 11.1 mmol mol^{-1} (average of 3.1 ± 1.1 mmol mol^{-1}) in shells from Rainbow, from 3.3 to 19.5 mmol mol^{-1} (average of 6.8 ± 3.4 mmol mol^{-1}) in shells from Menez Gwen, and from 2.8 to 4.5 mmol mol^{-1} (average of 3.4 ± 0.4 mmol mol^{-1}) in shells from EPR 9°50N (Fig. 3). We observe highly significant differences in shell Mg/Ca between sites (Kruskal and Wallis test, $p < 0.01$). Similarly, we note significant differences between habitats within both

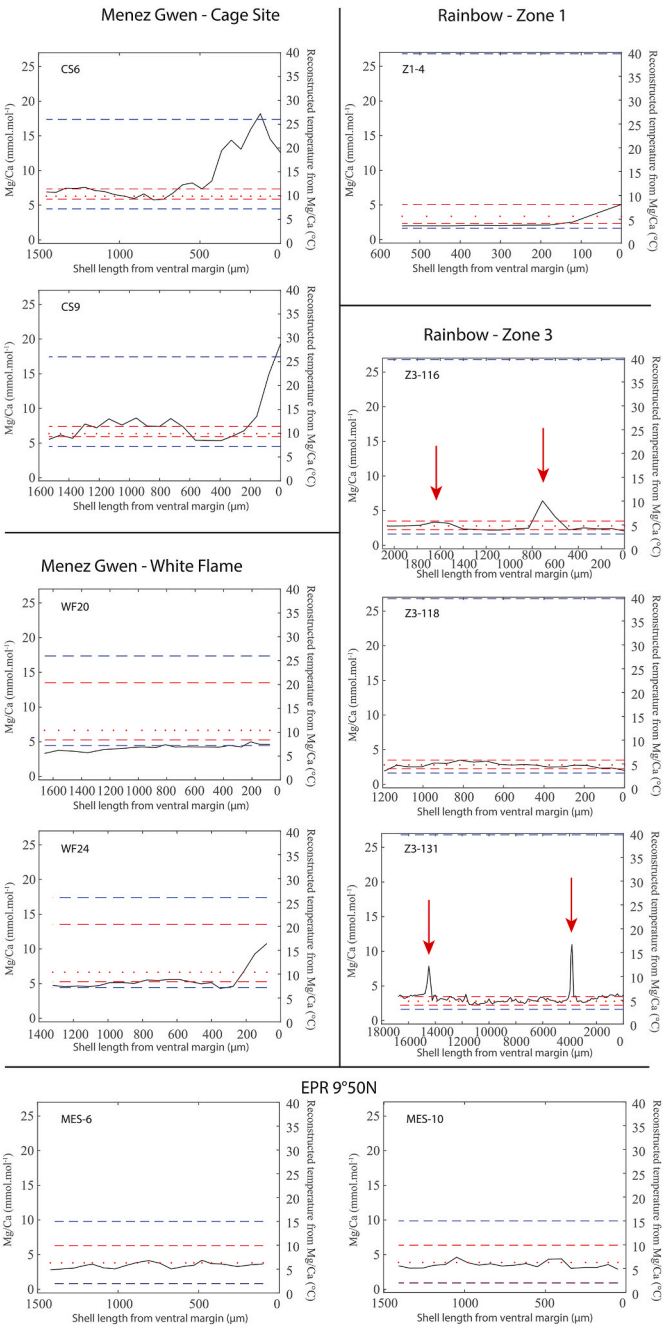

Fig. 3. Shell Mg/Ca and corresponding estimated temperatures. For each habitat, recorded temperature ranges are indicated by the red dashed lines and the average temperature in red dotted lines (this study; EPR: Nedoncelle et al., 2015). The historical temperature ranges, measured at each hydrothermal site, are indicated by the blue dashed lines (Rainbow: Desbruyères et al., 2001; Sarrazin et al., 2020; Menez Gwen: Colaço et al., 1998; Sarradin et al., 1999; Desbruyères et al., 2001; Sarrazin et al., 2020; EPR 9°50N: Mills et al., 2007; Moore et al., 2009; Luther et al., 2012). The red arrows correspond to the positions of major growth lines. (For interpretation of the references to colour in this figure legend, the reader is referred to the Web version of this article.)

Menez Gwen and Rainbow (Kruskal and Wallis test, $p < 0.01$).

The temperatures for Rainbow, estimated from Mg/Ca in the shells, range from 3.5 to 16.7 °C (average of 5.3 ± 1.5 °C). These calculated temperatures are quite stable (variation of ~1 °C) with the exceptions of one very localized peak at 10.1 °C in the shell Z3-116 and two thin peaks above 12 °C in the shell Z3-131 (Fig. 3). For each shell, these values are close similar to temperatures measured in the mussel habitat, showing an average of 5.6 ± 0.9 °C in Z1 mussel habitat and 4.8 ± 0.4 °C in Z3 habitat (Table 1, Fig. 3).

The estimated temperatures from the Menez Gwen shells range from 5.6 to 28.8 °C (average of 10.7 ± 4.8 °C) (Fig. 3). The two shells from Cage Site exhibit the same pattern with a slight variability in the estimated temperatures (between 8.4 and 13.5 °C) before a strong increase at the end of the deployment period (close to the shell ventral margin), with temperatures over 25 °C. We observe a similar pattern at White Flame for shell WF-24, which shows a relatively stable estimated temperature (between 7.0 and 8.9 °C) before an increase up to 16.4 °C at the end of the profile. However, shell WF-20 does not exhibit such an increase of estimated temperature, which remains between 5.6 and 8.0 °C across the transect.

For EPR 9°50N, both shells exhibit the same relatively stable estimated temperatures, ranging from 4.9 to 6.9 °C and from 4.9 to 7.4 °C, for MES6 and MES10, respectively.

The shell Z3-131, from Rainbow vent site, displays two major growth anomalies, close similar to the major growth lines (based on the description of major growth line made by Schöne and Giere (2005) in *Bathymodiolus brevior* and by Nedoncelle et al. (2014) in *B. azoricus* shells). These growth breaks are associated with the two peaks of Mg/Ca (Fig. 3). For both, the Mg/Ca values increased just before the occurrence of the major growth line (following the direction of growth), reaching the maximum values in the major growth line, and fall to the baseline values after. Two major growth lines were also detected in Z3-116 and one of these (M1, see Fig. 2) corresponds to a Mg/Ca peak (Fig. 3).

At Menez Gwen, the two shells from Cage Site, as well as shell specimen WF24 from White Flame, displayed a significant increase in Mg/Ca at the end of the profile (Fig. 3), but no major growth line was clearly observed. Nevertheless, the staining experiment revealed an absence of mineralization during the last 10 days of life (Supplementary Fig. S1), likely suggesting the formation of a growth stop (i.e., a major growth line) at this period. Thus Mg/Ca increase would anticipate the growth line formation as observed for Z3-116 and Z3-131 (Fig. 3). No major growth lines were detected in the shells from EPR 9°50N.

3.2. Oxygen stable isotope ratios

The measured $\delta^{18}O_w$ at Rainbow range from 0.05‰ (SMOW) at Z3 to 0.27‰ (SMOW) at Z1. Due to the lack of data in mussel beds at Menez Gwen and its proximity to Rainbow vent field, we assume a mean value of 0.16‰ (SMOW) for mussel habitats at Menez Gwen. The measurements in water surrounding mussels from EPR 9°50N gives a $\delta^{18}O_w$ value of −0.44‰ (SMOW).

Shells from Rainbow present $\delta^{18}O$ values between −1.37 and 4.12‰ (VPDB), and exhibit significant differences between ($p < 0.01$) and within habitats (Z1-7 different from Z1-1 and Z1-4: $p < 0.01$; Z3-131 different from A3-LIV4 and Z3-118: $p < 0.01$). Shells from Menez Gwen range from 2.52 to 3.91‰. A significant difference between shells between ($p < 0.01$) and within each habitat is also observed (WF-24 different from WF-20 and WF-22: $p < 0.01$; CS-4 different from CS-7: $p < 0.01$). $\delta^{18}O$ of shells from EPR 9°50N range from 2.21 to 4.27‰, and show no significant difference between shells from this site ($p = 0.57$). We also note a significant difference between sites ($p < 0.01$).

Reconstructed temperatures from each shell are presented in Fig. 4. The estimated temperatures are mostly lower than those measured on site (Fig. 4; Table 2). At Rainbow, two shells from Zone 1 present estimated temperatures lower than the measured *in situ* temperature range (mean estimates at 2.3 °C and 2.9 °C respectively, while mean measured temperature is 5.6 °C), along with some values below 0 °C, and only one shell (Z1-7) harbors reconstructed values in agreement with measured temperatures (mean estimated temperature: 5.2 °C; Fig. 4). For the Zone 3 of Rainbow, except for two values from one shell (A3-LIV4) which give estimated temperatures within the range of measured temperatures, the rest of reconstructed temperatures are below the minimum recorded temperature, with some negative values. All estimated temperatures

Table 1
Reconstructed temperatures from shell Mg/Ca compared to measured temperatures on study sites.

Site	Habitat	Sample	Estimated temperature (°C)		Measured temperature (°C), this study		Measured temperature (°C), literature	
			mean ± SD	min - max	mean ± SD	min - max	min – max	references
Rainbow	Z1	Z1-4	4.4 ± 1.5	3.6–8.1	5.6 ± 0.9	4.1–8.1	3.1–39.7	Desbruyères et al. (2001)
	Z3	Z3-116	4.8 ± 1.5	3.8–10.1	4.8 ± 0.4	4.0–5.8		Sarrazin et al. (2020)
		Z3-118	4.7 ± 0.6	3.5–5.8				
		Z3-131	5.5 ± 1.6	4.0–16.7				
Menez Gwen	Cage Site	CS-6	14.0 ± 5.3	9.1–27.2	9.9 ± 0.2	9.3–11.4	7.2–26.0	Colaço et al. (1998)
		CS-9	12.3 ± 5.0	8.4–28.8				Sarradin et al. (1999)
	White Flame	WF-20	6.8 ± 0.6	5.6–8.0	10.4 ± 3.1	8.4–20.4		Desbruyères et al. (2001)
		WF-24	8.9 ± 2.4	7.0–16.4				Meier et al. (2016)
								Sarrazin et al. (2020)
EPR 9°50N	V-vent	MES-6	5.8 ± 0.6	4.9–6.8	6.3 ± 2.1	2.0–9.9	2.0–15.0	Mills et al. (2007)
		MES-10	5.8 ± 0.7	4.9–7.4				Moore et al. (2009)
								Luther et al. (2012)

from shells of Menez Gwen are considerably less than the minimum measured on site, with occasionally negative reconstructed temperatures at Cage Site.

Only one value of estimated temperatures from shells of EPR 9°50N is above 0 °C. All others are significantl below the measured temperatures.

4. Discussion

4.1. Mg/Ca of bivalve shells as a possible thermometer proxy in hydrothermal settings

Within an error of ~1 °C, the skeletal Mg/Ca ratios in *B. azoricus* and *B. thermophilus* allow a reliable reconstruction of the average temperatures measured in the mussel habitat of the investigated vent sites, from the Atlantic and Pacific ridges (Table 1; Fig. 3). Although established with a shallow-water mussel species, the equation from Vander Putten et al. (2000) appears suitable to estimate temperatures using Mg/Ca ratios of deep-sea mussel shells. This is presumably due to (i) similar mineralogical and microstructural shell organisation of the two mytilid groups (Génio et al., 2012; Checa et al., 2014) and (ii) the specificity of geochemical conditions in these ecosystems. Far from the main continental inputs of Mg, the mussels used a stable supply of Mg from seawater to form their shells as the hydrothermal fluids are depleted in Mg (Charlou et al., 2002). Based on this assertion, the distribution coefficient of Mg^{2+} into the calcite material is strongly influenced by temperature changes. Thus, the difference observed between shells from the vent sites rely mainly on the different temperature conditions.

As reported for shallow-water mussel species (Lorens and Bender, 1980), the Mg/Ca ratio does not change in relation to growth variations in *Bathymodiolus* shells. An ontogenic trend in Mg/Ca was however described for different bivalve species (Freitas et al., 2005; Schöne et al., 2011; Mouchi et al., 2013). This could explain why the specimen Z3-131, the smallest shell from Rainbow, exhibits the highest Mg/Ca values among the shells on this site (Fig. 3). But this 'age effect' should have a lower influence in regard to temperature as specimen CS9 from Menez Gwen is in the same size range than the specimens from Rainbow, with clearly higher Mg/Ca ratios, and shells from EPR 9°50N exhibit similar values to shells from Rainbow while three times bigger. A better ontogenic growth profile for this species is however needed as growth rates can change according to the local environmental conditions (Nedoncelle et al., 2013).

Except for rare peaks, the reconstructed temperatures are quite stable at Rainbow (within ~1 °C variation), which is consistent with the measurements done at this site. At Menez Gwen – Cage Site habitat, before the large increase at the end of both shell profiles close to the ventral margin, that might be related to a specific process (see below), the estimated temperatures show more variability, with ~5 °C range. This variability is higher compared to our measurements done at this site during 10 days, but close to the temperature changes observed on long-term monitoring at Lucky Strike, the closest known site to Menez Gwen, and could refer to the lunar and two lunar periodicities identified there (Sarrazin et al., 2014). The lunar-related temperature dynamic is typically observed in *Bathymodiolius* sp. habitats (Khripounoff et al., 2008; Nedoncelle et al., 2015). Similarly, at White Flame, the reconstructed temperatures (i.e., 5.6–8.9 °C when final increase of WF-24 shell is avoided) should reflect the environmental periodicity of temperatures. The range of values are however slightly underestimated compared to the discrete measured temperature from this study during the Menez-MAR cruise (8.4–20.4 °C), but are close similar to the minimum recorded from other studies on this vent site (i.e., 7.2°C; Colaço et al., 1998).

Short-term peaks of Mg/Ca are however observed in some shells, and seems to be related to the formation of major growth breaks (called major growth lines in Schöne and Giere, 2005). The corresponding estimated temperatures increase reaches up to 17 °C at Rainbow and 29 °C at Menez Gwen, consistent with the maximum values measured at these sites (Table 1; Sarradin et al., 1999; Sarrazin et al., 2020). The maximum temperature recorded in the major growth lines can be however slightly overestimated due to possible high Mg concentrations in the shell organic matrix (Rosenberg and Hughes, 1991; Takesue et al., 2008; Lartaud et al., 2010b; Pérez-Huerta et al., 2020). Formation of shell organic matrix in biogenic carbonates is rich in sulfur, either as sulphated polysaccharides or S-rich amino acids, and for some species distribution of Mg correlates with S variability (Lorens and Bender, 1980; England et al., 2006; Foster et al., 2008). Some shells (WF-24, CS-6, CS-9, Z1-4) display a rise of Mg/Ca in the most recent shell parts (near collection date). This increase may correspond to the current formation of major growth lines, as we noted an absence of shell growth from calcein labels 10 days prior collection (Supplementary Fig. S1).

Different factors can act on Mg/Ca of bivalve shells, including the physiology of the organism which seems to generate breakdowns in the control of temperature on the incorporation of Mg, as illustrated for the mussel *M. edulis* (Vander Putten et al., 2000) and the oyster *Magallana gigas* (Mouchi et al., 2013). Although these types of breakdowns are not yet identified in deep-sea mussels, we cannot preclude their existence and further studies are required before applying directly the equation of Vander Putten et al. (2000) to reconstruct temperature changes in hydrothermal vent habitats.

4.2. Oxygen isotope ratios from hydrothermal vent mussels are unreliable temperature proxies

In contrast to Mg/Ca data, $\delta^{18}O$-inferred temperatures are underestimated, with values generally near or below 0 °C, which are unrealistic in these settings. Only one shell from Z1 presents reconstructed values close to the temperature measurements. All other shells from the different sites and habitats present reconstructed temperatures significantly lower than the minimum *in situ* temperature (Fig. 4). The

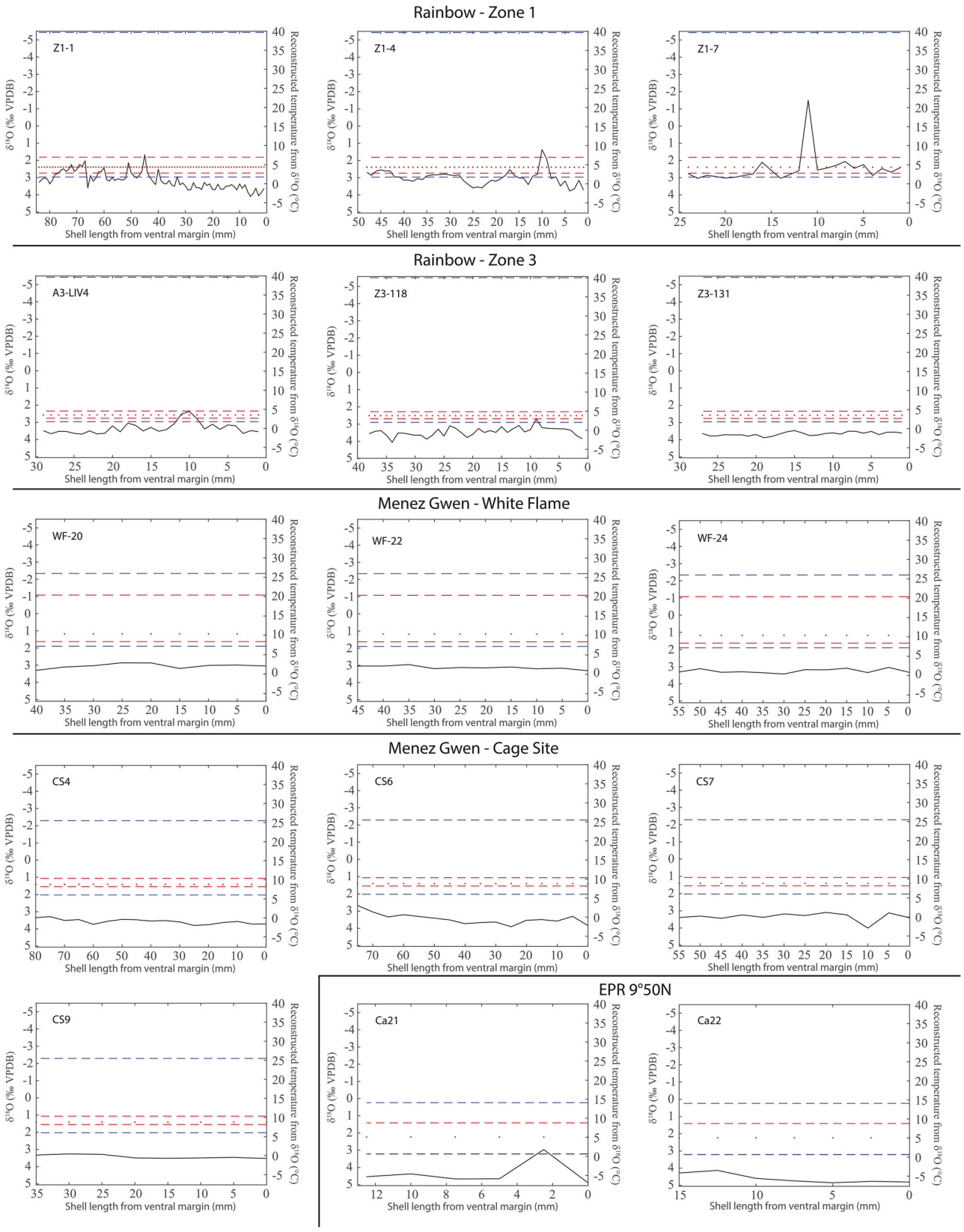

Fig. 4. Shell $\delta^{18}O$ and corresponding estimated temperatures. For each habitat, recorded temperature ranges are indicated by the red dashed lines and the average temperature in red dotted lines (this study; EPR: Nedoncelle et al., 2015). The historical temperature ranges measured at each hydrothermal site are indicated by the blue dashed lines (Rainbow: Desbruyères et al., 2001; Sarrazin et al., 2020; Menez Gwen: Colaço et al., 1998; Sarradin et al., 1999; Desbruyères et al., 2001; Sarrazin et al., 2020; EPR 9°50N: Mills et al., 2007; Moore et al., 2009; Luther et al., 2012). (For interpretation of the references to colour in this figure legend, the reader is referred to the Web version of this article.)

Table 2
Reconstructed temperatures from shell $\delta^{18}O$ compared to measured temperatures on study sites.

Site	Habitat	Sample	Estimated temperature (°C)		Measured temperature (°C), this study		Measured temperature (°C), literature	
			mean ± SD	min - max	mean ± SD	min - max	min – max	references
Rainbow	Z1	Z1-1	2.3 ± 2.1	−1.8 – 8.7	5.6 ± 0.9	4.1–8.1	3.1–39.7	Desbruyères et al. (2001)
		Z1-4	2.9 ± 1.9	−0.4 – 10.1				Sarrazin et al. (2020)
		Z1-7	5.2 ± 3.9	2.8–22.6				
	Z3	A3-LIV4	1.5 ± 1.5	−0.1 – 5.7	4.8 ± 0.4	4.0–5.8		
		Z3-118	0.7 ± 1.1	−2.0 – 3.9				
		Z3-131	0.1 ± 0.5	−0.9 – 0.9				
Menez Gwen	Cage Site	CS-4	0.5 ± 0.6	−0.5 – 1.7	9.9 ± 0.2	9.3–11.4	7.2–26.0	Colaço et al. (1998)
		CS-6	1.0 ± 1.3	−1.0 – 4.4				Sarradin et al. (1999)
		CS-7	1.5 ± 1.0	−1.4 – 2.5				Desbruyères et al. (2001)
		CS-9	1.1 ± 0.5	0.7–1.8				Meier et al. (2016)
	White Flame	WF-20	2.1 ± 0.6	1.0–2.9	10.4 ± 3.1	8.4–20.4		Sarrazin et al. (2020)
		WF-22	1.7 ± 0.4	0.9–2.5				
		WF-24	1.2 ± 0.5	0.4–2.1				
EPR 9°50N	V-vent	Ca21	−2.9 ± 3.1	−5.3 – 3.1	6.3 ± 2.1	2.0–9.9	2.0–15.0	Mills et al. (2007)
		Ca22	−4.0 ± 1.2	−5.1−−2.0				Moore et al. (2009)
								Luther et al. (2012)

measured values of $\delta^{18}O_w$, required to convert shell $\delta^{18}O$ into temperatures, may be a source of uncertainty if this parameter fluctuates outside the sampling period. Based on Kim and O'Neil (1997) equation, the $\delta^{18}O_w$ value expected to reconstruct accurate temperatures from shell $\delta^{18}O$ can be inferred. The expected values at both sites of Rainbow (0.55 and 0.71‰ at Z1 and Z3, respectively) are slightly higher than those measured (0.05‰ and 0.27‰, respectively), but within the known $\delta^{18}O_w$ from Rainbow, which range linearly from 0‰ (seawater) to ~1‰ (hydrothermal fluid) (Andreani et al., 2014). However, such $\delta^{18}O_w$ values would correspond to a mixing of >50 % of end-member fluid, leading to a temperature of ~180 °C if we assume temperature of hydrothermal fluids reaching 365 °C at Rainbow (Charlou et al., 2002), which is unlikely for an area suitable for mussels. The expected $\delta^{18}O_w$ values at Menez Gwen (White Flame and Cage Site habitats) and EPR 9°50N are substantially higher (1.91, 1.97 and 1.74‰, respectively). These values are largely above the current measured or estimated values for this site (i.e., 0.16 and −0.44‰ at Menez Gwen and EPR 9°50N, respectively). They also exceed $\delta^{18}O_w$ reports from Menez Gwen hydrothermal end-member (1.17 ± 0.06‰) (Jean-Baptiste et al., 1997) but are close to the higher values recorded in the hydrothermal fluids from EPR 9–10°N (0.6–1.9 ‰) (Shanks et al., 1991). Still, the corresponding conditions for such $\delta^{18}O_w$ values surrounding mussels would reach a mixing with >90 % of end-member, thus a temperature of ~347 °C if we assume temperature of hydrothermal fluids reaching 390 °C at EPR 9°50N (Proskurowski et al., 2008), far above the tolerance limit values of temperature for *Bathymodiolus* observed experimentally (i.e., 25–30°C, Boutet et al., 2009). A wrong estimation of $\delta^{18}O_w$ cannot therefore explain the discrepancy in reconstructed temperatures from shell $\delta^{18}O$.

Based on measured temperatures and $\delta^{18}O_w$ at sampling sites, the expected value of shell $\delta^{18}O$ at equilibrium with the environment was done using the equation of Kim and O'Neil (1997), and compared to the median shell $\delta^{18}O$ values. The resulting difference corresponds to the oxygen isotope disequilibrium (Table 3). *Bathymodiolus azoricus* from Rainbow are closer to isotopic equilibrium (i.e., mean disequilibrium of 0.28‰ and 0.66‰ for Z1 and Z3 habitats, respectively) than the shells from the other sites (disequilibrium of 1.75 ‰ for *B. azoricus* shells from White Flame and 1.81 ‰ for the ones from Cage Site, and 2.18‰ for *B. thermophilus* from EPR 9°50N). Such disequilibrium could be related to the influence of pH on oxygen isotope composition in biogenic carbonates (Usdowski et al., 1991; Kim and O'Neil, 1997; Zeebe, 1999). Particularly at hydrothermal vents, pH can greatly change with time and location, leading to a range of pH of 6.2–8 in *Bathymodiolus* habitats on the MAR and the EPR (Desbruyères et al., 2001; Kádár et al., 2005; Nedoncelle et al., 2015). Although bivalves can regulate their internal pH, it is estimated that this process is lower compared to other calcifying species such as corals, foraminifera and coralligenous algae, with an up-regulation limited to 0.5 pH unit (Crenshaw and Neff, 1969; Ip et al., 2006; McConnaughey and Gillikin, 2008).

Using the model described by Zeebe (2007), we reconstructed potential oxygen isotope disequilibrium induced by several pH scenarios (Table 4), in order to evaluate the impact of this parameter on shell $\delta^{18}O$. To do this, we considered salinity to be 34.7 at the EPR and 35 at the MAR vent sites (Haalboom et al., 2020). The oxygen isotope disequilibrium was tested for different pH scenarios and relative to a maximum pH of 8 (i.e., pH of deep seawater, Nedoncelle et al., 2015). At Rainbow, the oxygen isotope disequilibrium estimated in Table 3 can be explained by relatively restricted decrease in pH values compared to deep seawater. A fractionation of 0.2–0.3 at Z1 habitat is consistent with pH values of 7.7 ± 0.3 measured in *Bathymodiolus* habitats at this site (Desbruyères et al., 2001). The disequilibrium observed at Z3 habitat however requires a mean pH of 7.2, which appears low compared to the *Bathymodiolus* environment. A stronger decrease in pH would be necessary to cause the high isotopic disequilibrium observed at both Menez Gwen and EPR 9°50N. Although a pH decrease (values up to 6.7) has been observed at Menez Gwen (Desbruyères et al., 2001) and could

Table 3
Shell oxygen isotope disequilibrium based from measured temperature and seawater $\delta^{18}O$. The indicated value of $\delta^{18}O$ disequilibrium is the difference between shell $\delta^{18}O$ and expected shell $\delta^{18}O$ at equilibrium.

Site	Measured mean temperature (°C)	Measured $\delta^{18}O_w$ (‰ SMOW)	Expected shell $\delta^{18}O$ at equilibrium (‰ VPDB)	Median measured shell $\delta^{18}O$ (‰ VPDB)	Shell $\delta^{18}O$ disequilibrium (‰ VPDB)
Rainbow – Z1	5.6	0.27	2.72	3.00	0.28
Rainbow – Z3	4.8	0.05	2.71	3.37	0.66
Menez Gwen – White Flame	10.4	0.16	1.41	3.16	1.75
Menez Gwen – Cage Site	9.9	0.16	1.53	3.34	1.81
EPR 9°50N	6.3	−0.44	1.83	4.01	2.18

Table 4
Impact of pH on $\delta^{18}O$ disequilibrium. The model of Zeebe (2007) was used to reconstruct the α parameter from the thermodependent equation of Kim and O'Neil (1997), from salinity (S), temperature (T) and various pH scenarios. Theoretical $\delta^{18}O$ from potential pH values were then calculated from the equation using α and the measured $\delta^{18}O_w$.

Site	S	T (°C)	pH	α	Theoretical shell $\delta^{18}O$ (VPDB)	$\delta^{18}O$ disequilibrium compared to deep seawater pH = 8 (VPDB)
Rainbow	35	5.6	8	1.0355	4.97	0.29
Z1			7.7	1.0358	5.26	3.31
			6.2	1.0389	8.27	
Rainbow	35	4.8	8	1.0358	5.00	0.24
Z3			7.7	1.0360	5.24	0.65
			7.2	1.0364	5.65	3.30
			6.2	1.0392	8.30	
Menez	35	9.9	8	1.0344	3.83	0.26
Gwen			7.7	1.0347	4.09	1.04
Cage			6.9	1.0355	4.87	1.43
Site			6.7	1,0359	5.25	3.10
			6.2	1.0376	6.93	
Menez	35	10.4	8	1.0343	3.71	0.26
Gwen			7.7	1.0346	3.97	1.03
White			6.9	1.0354	4.74	1.42
Flame			6.7	1.0358	5.13	3.09
			6.2	1.0375	6.80	
EPR	34.7	6.3	8	1.0354	4.13	0.24
9°50N			7.7	1.0356	4.37	1.05
			6.9	1.0364	5.17	2.04
			6.5	1.0375	6.16	3.23
			6.2	1.0387	7.36	

explain a disequilibrium of 1.43 (Table 4), closer but still below to the ones described in Menez Gwen habitats (Table 3), it is unlikely mussels experienced such low pH values continuously. Other discrete measures in *Bathymodiolus* habitats from Menez Gwen exhibited pH values of 6.9 (Kádár et al., 2005), leading to a disequilibrium of ~1 while the current fractionation is > 1.7. Thus another factor would explain the high $\delta^{18}O$ values observed in mussel shells from this site. Similarly, at EPR 50°N continuous measurements show that pH range between 6.9 and 8, leading to a maximum disequilibrium of 1.05 (Table 4). To reach an oxygen isotope disequilibrium >2 as observed in Table 3, pH should decrease to 6.5, which is not consistent with the living conditions of this species there. It is thus unlikely that pH mainly controls shell $\delta^{18}O$ at Menez Gwen and EPR 9°50N.

Another potential influencing factor of stable isotope composition in shells is chemosynthesis, as already shown for $\delta^{13}C$ of *Bathymodiolus* (Nedoncelle et al., 2014). The sulfur-oxidizing symbionts provide CO_2 fixation in the Calvin-Benson cycle by the use of the RuBisCo enzyme. This enzyme favors light carbon incorporation in the organic tissues (Robinson and Cavanaugh, 1995; Fiala-Médioni et al., 2002), resulting in an enriched ^{13}C availability in the extrapallial cavity and thus in the shell. As they use carbon from methane rather than dissolved inorganic carbon from seawater as source of carbon, methanotroph symbionts have lower effect on the ^{13}C used for mineralization, leading to produce shells closer to isotopic equilibrium (Nedoncelle et al., 2014). Such effect on $\delta^{18}O$ was however never described for hydrothermal vent shells, although RuBisCo was also shown to induce oxygen isotope fractionation in cyanobacteria, photosynthetic bacteria and high-level plants, in favor of ^{16}O (Guy et al., 1993; Helman et al., 2005). An offset on oxygen isotopes occurs during microbial oxidation of sulfide (Markovic et al., 2016), which can lead to higher $\delta^{18}O$ values for the water pool used by the host organisms. The sulfur-oxidizing symbiont activity thus might additionally explain the positive disequilibrium measured on $\delta^{18}O$ of shells. Interestingly, contrary to the shells from Rainbow, shells from Menez Gwen (partly) and EPR 9°50N (mostly) have $\delta^{18}O$ values far from the isotopic equilibrium (Table 3), likely corresponding to a higher proportion of sulfur-oxidizing symbionts. This is consistent with the known repartition of symbionts in these mussel populations. *Bathymodiolus thermophilus* from EPR 9°50N rely only on sulfur-oxidizing symbionts and *B. azoricus*, which can harbor a dual symbiosis of sulfur-oxidizing and methanotrophs, exhibit a higher contribution to sulfo-oxidizing bacteria at Menez Gwen compared to Rainbow (Duperron et al., 2006; Halary et al., 2008; Nedoncelle et al., 2014).

5. Conclusion

Investigation of the Mg/Ca-temperature relationship in hydrothermal mussel shells reveals this proxy as a promising paleotemperature tracer for deep-sea species. This is the first suitability report of this proxy in deep-sea ecosystems, and although limited to hydrothermal vents, numerous applications of Mg/Ca analyses can be listed both with ecological and geological perspectives. Estimation of temperatures based on shell material will provide complementary tools to the direct measurements made by *in situ* probes, useful for the reconstruction of temperature changes at hydrothermal vents both over short-term (daily) and long-term (pluri-annual) scales. Although this relationship needs to be investigated deeper in details, deep-sea mussels, as they inhabit various ecosystems (*e.g.*, hydrothermal vents, cold seeps) seem to be a promising archive of long-term trends in deep-seawater temperatures. As such, they would give important information for oceanographic current modifications, as well as monitoring of fluid emissions.

On the contrary, $\delta^{18}O$ provides under-estimated temperatures. Although more study should be undertaken to explain this observation, pH variations on site may explain a substantial part of the isotopic disequilibrium. Still, we hypothesize that the type of symbiotic chemosynthetic bacteria has a strong impact on the oxygen isotope disequilibrium of their host's shell.

Finally, the results also show great benefits in the ecological study of vent mussels, particularly to determine temperature variations in the habitat and identify the response of biodiversity to thermal anomalies. This will give clues to better describe the ecological features of those species living in inaccessible habitats.

CRediT authorship contribution statement

V. Mouchi: Writing – review & editing, Writing – original draft, Visualization, Validation, Investigation, Formal analysis. **K. Nedoncelle:** Writing – review & editing, Methodology, Investigation, Formal analysis. **O. Bruguier:** Writing – review & editing, Validation, Methodology, Formal analysis. **Z. Garmirian:** Writing – review & editing, Investigation. **N. Le Bris:** Writing – review & editing, Supervision, Funding acquisition. **F. Lartaud:** Writing – review & editing, Writing – original draft, Visualization, Validation, Supervision, Project administration, Methodology, Investigation, Formal analysis, Data curation, Conceptualization.

Declaration of competing interest

The authors declare the following financial interests/personal relationships which may be considered as potential competing interests: Nadine Le Bris reports financial support was provided by TOTAL Foundation. If there are other authors, they declare that they have no known competing financial interests or personal relationships that could have appeared to influence the work reported in this paper.

Acknowledgements

We kindly thank captain and crew of the R/V L'Atalante and R/V Meteor, as well as the Nautile submersible, ROV Victor 6000 and Quest 4000 operation groups. The chief scientists of the research expeditions MoMARDREAM (J. Dyment, CNRS) and MenezMAR (N. Dubillier, MARUM), and the scientific parties are gratefully acknowledged for

their support and help during the cruises. The study benefited from the joint support of Fondation TOTAL and UPMC to the chair "Biodiversity, extreme marine environment and global change" (PI N. Le Bris) and from the financial support of the CNRS and the Institute of Ecology and Environment (INEE) to the UMR8222 LECOB for participation to the cruises and equipments. K Nedoncelle's PhD grant was funded by the French Ministry of Higher Education, Research and Innovation through the Doctoral School 'Sciences de l'Environnement d'Ile de France – ED129'. We also acknowledge L. Contreira Pereira for deployment of the temperature autonomous sensors at Menez Gwen – Cage Site and Charles Vidoudez for providing discrete temperature measurements at Menez Gwen - White Flame. Finally, we acknowledge the two anonymous reviewers who contributed to improve the manuscript.

Appendix A. Supplementary data

Supplementary data to this article can be found online at https://doi.org/10.1016/j.dsr.2025.104485.

Data availability

Data will be made available on request.

References

Aharon, P., 1991. Recorders of reef environment histories: stable isotopes in corals, giant clams and calcareous algae. Coral Reefs 10, 71–90.
Andreani, M., Escartin, J., Delacour, A., Ildefonse, B., Godard, M., Dyment, J., Fallick, A. E., Fouquet, Y., 2014. Tectonic structure, lithology, and hydrothermal signature of the Rainbow massif (Mid-Atlantic Ridge 36°14′N). G-cubed 15 (9), 3543–3571.
Boutet, I., Tanguy, A., Le Guen, D., Piccino, P., Hourdez, S., Legendre, P., Jollivet, D., 2009. Global depression in gene expression as a response to rapid thermal changes in vent mussels. Proc. Roy. Soc. Lond. B 276, 3071–3079.
Carré, M., Bentaleb, I., Bruguier, O., Ordinola, E., Barret, N.T., Fontugne, M., 2006. Calcification rate influence on trace element concentrations in aragonitic bivalve shells: evidence and mechanisms. Geochem. Cosmochim. Acta 70, 4906–4920.
Carter, J.G., 1980. Guide to bivalve shell microstructures. In: Rhoads, D.C., Lutz, R.A. (Eds.), Skeletal Growth of Aquatic Organisms. Plenum Press, New York, pp. 645–673.
Carter, J.G., 1990. Evolutionary significance of shell micro- structure in the Palaeotaxodonta, Pteriomorphia and Isofilibranchia. In: Carter, J.G. (Ed.), Skeletal Biomineralization: Patterns, Processes, and Evolutionary Trends, vol. I. Van Nostrand Reinhold, New York, USA, pp. 135–296.
Charlou, J.L., Donval, J.P., Fouquet, Y., Jean-Baptiste, P., Holm, N., 2002. Geochemistry of high H2 and CH4 vent fluids issuing from ultramafic rocks at the Rainbow hydrothermal field (36°14'N, MAR). Chem. Geol. 191, 345–359.
Checa, A.G., Pina, C.M., Osuna-Mascaro, A.B., Harper, E.M., 2014. Crystalline organization of the fibrous prismatic calcitic layer of the Mediterranean mussel *Mytilus galloprovincialis*. Eur. J. Mineral 26, 495–505.
Colaço, A., Desbruyères, D., Comtet, T., Alayse, A.M., 1998. Ecology of the Menez gwen hydrothermal vent field (Mid-Atlantic Ridge/azores triple junction). Cah. Biol. Mar. 39, 237–240.
Coplen, T.B., Kendall, C., Hopple, J., 1983. Comparison of stable isotope reference samples. Nature 302 (5905), 236–238.
Corliss, J.B., Dymond, J., Gordon, L.I., Edmond, J.M., von Herzen, R.P., Ballard, R.D., Green, K., Williams, D., Bainbridge, A., Crane, K., van Andel, T.H., 1979. Submarine thermal springs on the galapagos rift. Science 203, 1073–1083.
Cravo, A., Foster, P., Almeida, A., Bebianno, M.J., Company, R., 2008. Metal concentrations in the shell of *Bathymodiolus azoricus* from contrasting hydrothermal vent fields on the mid-Atlantic ridge. Mar. Environ. Res. 65, 338–348.
Crenshaw, M.A., Neff, J.M., 1969. Decalcification at the mantle-shell interface in molluscs. Am. Zool. 9, 881–885.
Daëron, M., Drysdale, R.N., Peral, M., Huyghe, D., Blamart, D., Coplen, T.B., Lartaud, F., Zanchetta, G., 2019. Most Earth-surface calcites precipitate out of isotopic equilibrium. Nat. Commun. 10, 429.
Demina, L.L., Holm, N.G., Galkin, S.V., Lein, A.Y., 2013. Some features of the trace metal biogeochemistry in the deep-sea hydrothermal vent fields (Menez Gwen, Rainbow, Broken Spur at the MAR and 9°50'N at the EPR): a synthesis. J. Mar. Syst. 126, 94–105.
Desbruyères, D., Biscoito, M., Caprais, J.C., Colaço, A., Comtet, T., Crassous, P., Fouquet, Y., Khripounoff, A., Le Bris, N., Olu, K., Riso, R., Sarradin, P.M., Segonzac, M., Vangriesheim, A., 2001. Variations in deep-sea hydrothermal vent communities on the Mid-Atlantic Ridge near the Azores plateau. Deep Sea Res. I 48, 1325–1346.
Dettman, D.L., Reische, A.K., Lohmann, K.C., 1999. Controls on the stable isotope composition of seasonal growth bands in aragonitic fresh-water bivalves (unionidae). Geochem. Cosmochim. Acta 63 (7/8), 1049–1057.
Dodd, J.R., 1965. Environmental control of strontium and magnesium in *Mytilus*. Geochem. Cosmochim. Acta 29, 385–398.
Duperron, S., Bergin, C., Zielinski, F., Blazejak, A., Pernthaler, A., McKiness, Z.P., DeChaine, E., Cavanaugh, C.M., Dubilier, N., 2006. A dual symbiosis shared by two mussel species, *Bathymodiolus azoricus* and *Bathymodiolus puteoserpentis* (Bivalvia: mytilidae), from hydrothermal vents along the northern Mid-Atlantic Ridge. Environ. Microbiol. 8, 1441–1447.
England, J., Cusack, M., Lee, M.R., 2006. Magnesium and sulphur in the calcite shells of two brachiopods, *Terebratulina retusa* and *Novocrania anomala*. Lethaia 40, 2–10.
Fiala-Médioni, A., McKiness, Z.P., Dando, P., Boulegue, J., Mariotti, A., Alayse-Danet, A. M., Robinson, J.J., Cavanaugh, C.M., 2002. Ultrastructural, biochemical, and immunological characterization of two populations of the mytilid mussel *Bathymodiolus azoricus* from the Mid-Atlantic Ridge: evidence for a dual symbiosis. Mar. Biol. 141, 1035–1043.
Foster, L.C., Finch, A.A., Allison, N., Andersson, C., Clarke, L.J., 2008. Mg in aragonitic bivalve shells: seasonal variations and mode of incorporation in *Arctica islandica*. Chem. Geol. 254, 113–119.
Freitas, P., Clarke, L.J., Kennedy, H., Richardson, C., Abrantes, F., 2005. Mg/Ca, Sr/Ca, and stable-isotope ($\delta^{18}O$ and $\delta^{13}C$) ratio profiles from the fan mussel *Pinna nobilis*: seasonal records and temperature relationships. Geochemistry Geophys. Geosystems 6, Q04D14.
Freitas, P.S., Clarke, L.J., Kennedy, H.A., Richardson, C.A., 2008. Inter- and intra-specimen variability masks reliable temperature control on shell Mg/Ca ratios in laboratory- and field-cultured *Mytilus edulis* and *Pecten maximus* (bivalvia). Biogeosciences 5, 1245–1258.
Freitas, P.S., Clarke, L.J., Kennedy, H., Richardson, C.A., 2012. The potential of combined Mg/Ca and $\delta^{18}O$ measurements within the shell of the bivalve *Pecten maximus* to estimate seawater $\delta^{18}O$ composition. Chem. Geol. 291, 286–293.
Génio, L., Kiel, S., Cunha, M.R., Grahame, J., Little, C.T.S., 2012. Shell microstructures of mussels (Bivalvia: mytilidae: Bathymodiolinae) from deep-sea chemosynthetic sites: do they have a phylogenetic significance? Deep Sea Res. I 64, 86–103.
Goodwin, D.H., Banker, R., Watters, G.T., Dettman, D.L., Romanek, C.S., 2019. Reconstructing intra-annual growth of freshwater mussels using oxygen isotopes. Chem. Geol. 526, 7–22. https://doi.org/10.1016/J.CHEMGEO.2018.07.030.
Guy, R.D., Fogel, M.L., Berry, J.A., 1993. Photosynthetic fractionation of the stable isotopes of oxygen and carbon. Plant. Physiol. 101, 37–47.
Haalboom, S., Price, D.M., Mienis, F., van Bleijswijk, J.D.L., de Stigter, H.C., Witte, H.J., Reichart, G.-J., Duineveld, G.C.A., 2020. Patterns of (trace) metals and microorganisms in the Rainbow hydrothermal vent plume at the Mid-Atlantic Ridge. Biogeosciences 17, 2499–2519.
Halary, S., Riou, V., Gaill, F., Boudier, T., Duperron, S., 2008. 3D FISH for the quantification of methane- and sulphur-oxidizing endosymbionts in bacteriocytes of the hydrothermal vent mussel *Bathymodiolus azoricus*. ISME J. 2, 284–292.
Helman, Y., Barkan, E., Eisenstadt, D., Luz, B., Kaplan, A., 2005. Fractionation of the three stable oxygen isotopes by oxygen-producing and oxygen-consuming reactions in photosynthetic organisms. Plant. Physiol. 138, 2292–2298.
Huyghe, D., Lartaud, F., Emmanuel, L., Merle, D., Renard, M., 2015. Palaeogene climate evolution in the Paris Basin from oxygen stable isotope ($\delta^{18}O$) compositions of marine molluscs. J. Geol. Soc. London. 172, 576–587.
Huyghe, D., Emmanuel, L., de Rafélis, M., Renard, M., Ropert, M., Labourdette, N., Lartaud, F., 2020. Oxygen isotope disequilibrium in the juvenile portion of oyster shells biases seawater temperature reconstructions. Estuar. Coast Shelf Sci. 240, 106777.
Huyghe, D., Daëron, M., de Rafelis, M., Blamart, D., Sébilo, M., Paulet, Y.-M., Lartaud, F., 2022. Clumped isotopes in modern marine bivalves. Geochem. Cosmochim. Acta 316, 41–58.
Ip, Y.K., Loong, A.M., Kiong, K.C., Wong, W.P., Chew, S.F., Reddy, K., Sivalonganathan, B., Ballantyne, J.S., 2006. Light induces an increase in the pH of and a decrease in the ammonia concentration in the extrapallial fluid of the giant clam *Tridacna squamosa*. Physiol. Biochem. Zool. 79, 656–664.
Jean-Baptiste, P., Charlou, J.L., Stievenard, M., 1997. Oxygen isotope study of mid-ocean ridge hydrothermal fluids: implications for the oxygen-18 budget of the oceans. Geochem. Cosmochim. Acta 61, 2669–2677.
Johnson, K.S., Childress, J.J., Beelher, C.L., Sakamoto, C.M., 1994. Biogeochemistry of hydrothermal vent mussel communities: the deep-sea analogue to the intertidal zone. Deep Sea Res. I 41, 993–1011.
Kádár, E., Costa, V., Martins, I., Santos, R.S., Powell, J.J., 2005. Enrichment in trace metals (Al, Mn, Co, Cu, Mo, Cd, Fe, Zn, Pb and Hg) of macro-invertebrate habitats at hydrothermal vents along the Mid-Atlantic Ridge. Hydrobiologia 548, 191–205.
Kenk, V.C., Wilson, B.R., 1985. A new mussel (Bivalvia, Mytilidae) from hydrothermal vents, in the Galapagos Rift zone. Malacologia 26 (1–2), 253–271.
Khripounoff, A., Vangriesheim, A., Crassous, P., Segonzac, M., Lafon, V., Warén, A., 2008. Temporal variation of currents, particulate flux and organism supply at two deep-sea hydrothermal fields of the Azores Triple Junction. Deep Sea Res. I 55, 532–551.
Kim, S.T., O'Neil, J.R., 1997. Equilibrium and nonequilibrium oxygen isotope effects in synthetic carbonates. Geochem. Cosmochim. Acta 61, 3461–3475.
Klein, R.T., Lohmann, K.C., Thayer, C.W., 1996. Bivalve skeletons record sea-surface temperature and $\delta^{18}O$ via Mg/Ca and $^{18}O/^{16}O$ ratios. Geology 24, 415–418.
Lartaud, F., Emmanuel, L., de Rafélis, M., Ropert, M., Labourdette, N., Richardson, C.A., Renard, M., 2010a. A latitudinal gradient of seasonal temperature variation recorded in oyster shells from the coastal waters of France and The Netherlands. Facies 56, 13–25.
Lartaud, F., de Rafelis, M., Oliver, G., Krylova, E., Dyment, J., Ildefonse, B., Thibaud, R., Gente, P., Hoisé, E., Meistertzheim, A.L., Fouquet, Y., Gaill, F., Le Bris, N., 2010b. Fossil clams from a serpentinite-hosted sedimented vent field near the active smoker

complex Rainbow (MAR, 26°13N): insight into the biogeography of vent fauna. Geochemistry Geophys. Geosystems 11, Q0AE01.
Lartaud, F., Little, C.T.S., de Rafelis, M., Bayon, G., Dyment, J., Ildefonse, B., Gressier, V., Fouquet, Y., Gaill, F., Le Bris, N., 2011. Fossil evidence for serpentinization fluids fueling chemosynthetic assemblages. Proc. Natl. Acad. Sci. U. S. A. 108, 7698–7703.
Le Bris, N., Duperron, S., 2010. Chemosynthetic communities and biogeochemical energy pathways along the Mid-Atlantic Ridge: the case of *Bathymodiolus azoricus*. Geophys. Monogr. 188, 409–429.
Le Bris, N., Yücel, M., Das, A., Sievert, S.M., LokaBharathi, P., Girguis, P.R., 2019. Hydrothermal energy transfer and organic carbon production at the deep seafloor. Front. Mar. Sci. 5, 531.
Lelièvre, Y., Legendre, P., Matabos, M., Mihaly, M., Lee, R.W., Sarradin, P.M., Arango, C. P., Sarrazin, J., 2017. Astronomical and atmospheric impacts on deep-sea hydrothermal vent invertebrates. Proc. R. Soc. – Biol. Sci. 284, 20162123.
Lietard, C., Pierre, C., 2009. Isotopic signatures ($\delta^{18}O$ and $\delta^{13}C$) of bivalve shells from cold seeps and hydrothermal vents. Geobios 42, 209–219.
Longerich, H.P., Gunther, D., Jackson, S.E., 1996. Elemental fractionation in laser ablation inductively coupled plasma mass spectrometry. Fresenius J. Anal. Chem. 355, 538–542.
Lopez-Correa, M., Montagna, P., Vendrell-Simon, B., McCulloch, M., Taviani, M., 2010. Stable isotopes ($\delta^{18}O$ and $\delta^{13}C$), trace and minor element compositions of Recent scleractinians and Last Glacial bivalves at the Santa Maria di Leuca deep-water coral province, Ionian sea. Deep Sea Res. II 57, 471–486.
Lorens, R.B., Bender, M.L., 1980. The impact of solution chemistry on *Mytilus edulis* calcite and aragonite. Geochem. Cosmochim. Acta 44, 1265–1278.
Luther, G.W., Gartman, A., Yücel, M., Madison, A.S., Moore, T.S., Nees, H.A., Nuzzio, D. B., Sen, A., Lutz, R.A., Shank, T.M., Fisher, C.R., 2012. Chemistry, temperature, and faunal distributions at diffuse-flow hydrothermal vents: comparison of two geologically distinct ridge systems. Oceanography (Wash., D.C.) 25, 234–245.
Lutz, R.A., Kennish, M.J., Pooley, A.S., Fritz, L.W., 1994. Calcium carbonate dissolution rates in hydrothermal vent fields of the Guaymas Basin. J. Mar. Res. 52, 969–982.
Machado, J., Lopes-Lima, M., Damasceno-Olivera, A., Colaço, A., Andrade, J., Silva, D., Jiménez-Lopez, C., Rodriguez-Navarro, A., Checa, A., 2009. The influence of hydrostatic pressure on shell mineralization of *Anodonta cygnea*: a comparative study with a hydrothermal vent bivalve *Bathymodiolus azoricus*. J. Shellfish Res. 28, 899–904.
Markovic, S., Paytan, A., Li, H., Wortmann, U.G., 2016. A revised seawater sulfate oxygen isotope record for the last 4 Myr. Geochem. Cosmochim. Acta 175, 239–251.
McConnaughey, T.A., Gillikin, D.P., 2008. Carbon isotopes in mollusk shell carbonates. Geo Mar. Lett. 28, 287–299.
Meier, D.V., Bach, W., Girguis, P.R., Gruber-Vodicka, H.R., Reeves, E.P., Richter, M., Vidoudez, C., Amann, R., Meyerdierks, A., 2016. Heterotrophic *Proteobacteria* in the vicinity of diffuse venting. Environ. Microbiol. 18, 4348–4368.
Mikkelsen, P.M., Bieler, R., Kappner, I., Rawlings, T.A., 2006. Phylogeny of Veneroidea (Mollusca: Bivalvia) based on morphology and molecules. Zool. J. Linn. Soc. 148, 439–521.
Mills, S.W., Mullineaux, L.S., Tyler, P.A., 2007. Habitat associations in gastropod species at East Pacific rise hydrothermal vents (9°50′N). Biol. Bull. 212, 185–194.
Moore, T.S., Shank, T.M., Nuzzio, D.B., Luther, G.W., 2009. Time-series chemical and temperature habitat characterization of diffuse flow hydrothermal sites at 9°50′N East Pacific Rise. Deep-Sea Research II 56, 1616–1621.
Mouchi, V., de Rafelis, M., Lartaud, F., Fialin, M., Verrecchia, E., 2013. Chemical labelling of oyster shells used for time-calibrated high-resolution Mg/Ca ratios: a tool for estimation of past seasonal temperature variations. Palaeogeogr. Palaeoclimatol. Palaeoecol. 373, 66–74.
Mouchi, V., Briard, J., Gaillot, S., Argant, T., Forest, V., Emmanuel, L., 2018. Reconstructing environments of collection sites from archaeological bivalve shells: case study from oysters (Lyon, France). J. Archaeol. Sci. Reports 21, 1225–1235.
Mullineaux, L.S., Le Bris, N., Mills, S.W., Henri, P., Bayer, S.R., Secrist, R.G., Siu, N., 2012. Detecting the influence of initial pioneers on succession at deep-sea vents. PLoS One 7, e50015.
Naraoka, H., Naito, T., Yamanaka, T., Tsunogai, U., Fujikura, K., 2008. A multi-isotope study of deep-sea mussels at three different hydrothermal vent sites in the northwestern Pacific. Chem. Geol. 255, 25–32.
Nedoncelle, K., Lartaud, F., de Rafelis, M., Boulila, S., Le Bris, N., 2013. A new method for high-resolution bivalve growth rate studies in hydrothermal environments. Mar. Biol. 160, 1427–1439.
Nedoncelle, K., Le Bris, N., de Rafelis, M., Labourdette, N., Lartaud, F., 2014. Non-equilibrium fractionation of stable carbon isotopes in chemosynthetic mussels. Chem. Geol. 387, 35–46.
Nedoncelle, K., Lartaud, F., Contreira Pereira, L., Yücel, M., Thurnherr, A.M., Mullineaux, L., Le Bris, N., 2015. *Bathymodiolus* growth dynamics in relation to environmental fluctuations in vent habitats. Deep Sea Res. I 106, 183–193.
Pearce, N.J.G., Perkins, W.T., Westgate, J.A., Gorton, M.P., Jackson, S.E., Neal, C.R., Chenery, S.P., 1997. A Compilation of New and Published Major and Trace Element Data for NIST SRM 610 and NIST SRM 612 Glass Reference Materials, vol. 21. Geostandard Newsletters, pp. 115–144.
Pérez-Huerta, A., Walker, S.E., Cappelli, C., 2020. In situ geochemical analysis of organics in growth lines of Antarctic scallop shells: implications for sclerochronology. Minerals 10, 529.
Pierre, C., Vangriesheim, A., Laube-Lenfant, E., 1994. Variability of water masses and of organic production-regeneration systems as related to eutrophic, mesotrophic and oligotrophic conditions in the northeast Atlantic ocean. J. Mar. Syst. 5, 159–170.
Proskurowski, G., Lilley, M.D., Olson, E.J., 2008. Stable isotopic evidence in support of active microbial methane cycling in low-temperature diffuse flows vents at 9°50′N East pacific Rise. Geochem. Cosmochim. Acta 72, 2005–2023.
Rio, M., Renard, M., Roux, M., Clauser, S., Davanzo, F., Herrerra, Duvault Y., 1988. Composition chimique et isotopique des tests de bivalves des sources hydrothermales océaniques. Bull. Soc. Geol. Fr. 9, 151–159.
Robinson, J.J., Cavanaugh, C.M., 1995. Expression of form I and form II ribulose-1,5-bisphosphate carboxylase/oxygenase (RuBsiCo) in chemoautotrophic symbioses: implications for the interpretation of stable carbon isotope ratios. Limnol. Oceanogr. 40, 1496–1502.
Robinson, L.F., Adkins, J.F., Frank, N., Gagnon, A.C., Prouty, N., Roark, E.B., van de Flierdt, T., 2014. The geochemistry of deep-sea coral skeletons: a review of vital effects and applications for palaeoceanography. Deep Sea Res. II 99, 184–198.
Rohling, E.J., 2000. Paleosalinity: confidence limits and future applications. Mar. Geol. 163, 1–11.
Rosenberg, G.D., Hughes, W.W., 1991. A metabolic model for the determination of shell composition in the bivalve mollusc, *Mytilus edulis*. Lethaia 24, 83–96.
Sarradin, P.M., Caprais, J.C., Riso, R., Kerouel, R., Aminot, A., 1999. Chemical environment of the hydrothermal mussel communities in the Lucky Strike and Menez gwen vent fields, Mid-Atlantic Ridge. Cah. Biol. Mar. 40, 93–104.
Sarrazin, J., Cuvelier, D., Peton, L., Legendre, P., Sarradin, P.M., 2014. High-resolution dynamics of a deep-sea hydrothermal mussel assemblage monitored by the EMSO-Açores MoMAR observatory. Deep Sea Res. I 90, 62–75.
Sarrazin, J., Portail, M., Legrand, E., Cathalot, C., Laes, A., Lahaye, N., Sarradin, P.M., Husson, B., 2020. Endogenous versus exogenous factors: what matters for vent mussel communities? Deep-Sea Res. 160, 103260.
Scheirer, D.S., Shank, T.M., Fornari, D.J., 2006. Temperature variations at diffuse and focused flow hydrothermal vent sites along the northern East Pacific Rise. Geochemistry Geophys. Geosystems 7, Q03002.
Schöne, B.R., 2008. The curse of physiology-challenges and opportunities in the interpretation of geochemical data from mollusk shells. Geo Mar. Lett. 28, 269–285.
Schöne, B.R., Giere, O., 2005. Growth increments and stable isotope variation in shells of the deep-sea hydrothermal vent bivalve mollusk *Bathymodiolus brevior* from the North Fiji Basin, Pacific Ocean. Deep Sea Res. I 52, 1896–1910.
Schöne, B.R., Pfeiffer, M., Pohlmann, T., Siegismund, F., 2005a. A seasonally resolved bottom-water temperature record for the period 1866-2002 based on shells of *Arctica islandica* (Mollusca, North Sea). Int. J. Climatol. 25, 947–962.
Schöne, B.R., Dunca, E., Fiebig, J., Pfeiffer, M., 2005b. Mutvei's solution: an ideal agent for resolving microgrowth structures of biogenic carbonates. Palaeogeogr. Palaeoclimatol. Palaeoecol. 228, 149–166.
Schöne, B.R., Zhang, Z., Radermacher, P., Thébault, J., Jacob, D., Nunn, E., Maurer, A.F., 2011. Sr/Ca and Mg/Ca ratios of ontogenetically old bivalve shells (*Arctica islandica*) and their function as paleotemperature proxies. Palaeogeogr. Palaeoclimatol. Palaeoecol. 302, 52–64.
Shanks III, W.C., Bohlke, J.K., Seal, R.R.I.I., 1991. Stable isotopes studies of vent fluids, 9-10°N East Pacific Rise: water- rock interaction and phase separation. EOS 72, 48.
Shirai, K., Takahata, N., Yamamoto, H., Omata, T., Sasaki, T., Sano, Y., 2008. Novel analytical approach to bivalve shell biogeochemistry: a case study of hydrothermal mussel shell. Geochem. J. 42, 413–420.
Surge, D., Lohmann, K.C., 2008. Evaluating Mg/Ca ratios as a temperature proxy in the estuarine oyster, *Crassostrea virginica*. J. Geophys. Res. Biogeosciences 113, G2001.
Takesue, R.K., Bacon, C.R., Thompson, J.K., 2008. Influences of organic matter and calcification rate in trace elements in aragonitic estuarine bivalve shells. Geochem. Cosmochim. Acta 72, 5431–5445.
Tanaka, K., Okaniwa, N., Miyaji, T., Murakami-Sugihara, N., Zhao, L., Tanabe, K., Schöne, B.R., Shirai, K., 2019. Microscale magnesium distribution in shell of the Mediterranean mussel *Mytilus galloprovincialis*: an example of multiple factors controlling Mg/Ca in biogenic calcite. Chem. Geol. 511, 521–532.
Tarutani, T., Clayton, R.N., Mayeda, T.K., 1969. The effect of polymorphism and magnesium substitution on oxygen isotope fractionation between calcium carbonate and water. Geochem. Cosmochim. Acta 33, 987–996.
Tivey, M.K., Bradley, A.M., Joyce, T.M., Kadko, D., 2002. Insights into tide-related variability at seafloor hydrothermal vents from time-series temperature measurements. Earth Planet Sci. Lett. 202, 693–707.
Tynan, S., Opdyke, B.N., Walczak, M., Eggins, S., Dutton, A., 2017. Assessment of Mg/Ca in *Saccostrea glomerata* (the Sydney rock oyster) shell as a potential temperature record. Palaeogeogr. Palaeoclimatol. Palaeoecol. 484, 79–88.
Urey, H.C., 1947. The thermodynamic properties of isotopic substances. Journal of Chemical Society 562–581.
Usdowski, E., Michaelis, J., Böttcher, M.E., Hoefs, J., 1991. Factors for the oxygen isotope equilibrium fractionation between aqueous and gaseous CO_2, carbonic acid, bicarbonate, carbonate, and water (19°C). Z. Phys. Chem. 170, 237–249.
Van Dover, C.L., 2000. The ecology of deep-sea hydrothermal vents. Princeton University Press.
Vander Putten, E., Dehairs, F., Keppens, E., Baeyens, W., 2000. High resolution distribution of trace elements in the calcite shell layers of modern *Mytilus edulis*: environmental and biological controls. Geochem. Cosmochim. Acta 64, 997–1011.
von, Cosel R., Comtet, T., Krylova, E.M., 1999. *Bathymodiolus* (Bivalvia: mytilidae) from hydrothermal vents from hydrothermal vents on the Azores triple junction and the Logatchev hydrothermal field. Veliger 42 (3), 218–248.
Wanamaker, A.D.J., Kreutz, K.J., Wilson, T., Borns, H.W.J., Introne, D.S., Feindel, S., 2008. Experimentally determined Mg/Ca and Sr/Ca ratios in juvenile bivalve calcite for *Mytilus edulis*: implications for paleotemperature reconstructions. Geo Mar. Lett. 28, 359–368.
Welsh, K., Elliot, M., Tudhope, A., Ayling, B., Chapell, J., 2011. Giant bivalves (*Tridacna gigas*) as recorders of ENSO variability. Earth Planet Sci. Lett. 307, 266–270.
Wisshak, M., Lopez Correa, M., Gofas, S., Salas, C., Taviani, M., Jakobsen, J., Freiwald, A., 2009. Shell architecture, element composition, and stable isotope

signature of the giant deep-sea oyster *Neopycnodonte zibrowii* sp. N. from the NE Atlantic. Deep-Sea Res. I 56, 374–407.
Zeebe, R.E., 1999. An explanation of the effect of seawater carbonate concentration on foraminiferal oxygen isotopes. Geochem. Cosmochim. Acta 63, 2001–2007.
Zeebe, R.E., 2007. An expression for the overall oxygen isotope fractionation between the sum of dissolved inorganic carbon and water. G-cubed 8, Q09002. https://doi.org/10.1029/2007GC001663.